Chapter 5

Monte Carlo Study of the Dosimetric Properties of an Unflattened 6-MV Photon Beam

ABSTRACT

Flattening Filter Free (FFF) photon beams have different dosimetric properties from those of flattened beams. This chapter reports on the basic dosimetric properties of a Flattening-filter-free 6-MV photon beam produced by Varian Clinic 600 linac (unique performance model) after removing the flattening filter from beam line. We carried out this simulation study of unflattened beam by removing the flattening filter from beam path in our simulation model. Dosimetric characteristics, including the central-axis absorbed dose, the beam profiles and the photon and electron fluences were calculated for both flattened and unflattened cases individually by using Monte Carlo simulations. Depth dose calculations showed an increase of more than twofold in the dose rate for the unflattened 6-MV photon beam which was depended on the depth. These results suggest that the removal of the filter from the beam line could result in higher central-axis dose rates and hence, shorter beam delivery times for treatment can be achieved. Removal of the filter from the beam line results in presence of more contaminates electrons and low-energy photons in the unflattened beam, due to which increased surface dose were found for the unflattened beam. Less variation in the total scatter factor (S_{CP}) with the field sizes indicates, that removing the filter from the beam line can reduce significantly the amount of head scatter photons and results in less dose to normal tissues and organs other than targeted. Our study of unflattened beam dose profiles showed that the dosimetric field size and penumbra were slightly smaller for them in compare to flattened beam. Increased dose rate and lower out of field dose could be considered as realistic advantages for unflattened photon beams.

5.1 INTRODUCTION

Traditional clinical linear accelerators are equipped with a flattening filter (FF). The principle intends of flattening filter is to produce a flat beam profile at a given depth by compensating for the non uniformity of photon fluence across the field. But flattening filter decreases the X-ray output considerably and produces quality changes within the primary beam by scattering and absorption of primary photons. The requirement to have a flattened beam profile for treatment delivery is no longer necessary for many types of treatments such as intensity-modulated radiation therapy or intensity-modulated arc therapy. In intensity modulated radiation therapy (IMRT), the patient dose distribution can instead be shaped by the multileaf collimator (MLC) to create the desired clinical effect. In principle, the flattening filter can then be removed, and the leaf sequences can be adjusted so to produce fluence distributions similar to those of a beam with a flattening filter. Recent research and the introduction of Flattening filter free beams to clinical practice has generated considerable interest in radiotherapy because of the advantages of unflattened beams as compared to traditional flattened beams. These advantages include removal of the flattening filter with its associated attenuation from the X-ray beam path, increases the dose rate **[Fu *et al.* (2004)]**. The other potential outcome is considerable reduction in head scatter, as the flattening filter is the major source of scattered photons. A decrease in head scatter will improve the dosimetry of unflattened beams, resulting in reduced output variation with the radiation field size and reduced variations in all field-size-dependent parameters. Flattening filter free (FFF) beams in radiotherapy thus have the advantage of shorter treatment delivery time and lower out-of field dose compared with conventional flattened beams. This is especially important where large doses per fraction are prescribed, e.g., stereotactic ablative body radiotherapy **[Gillies *et***

***al.* (1993), O'Brien *et al.* (1991)]** or where patient motion might affect the efficacy of the delivery or both **[Jeraj *et al.*(2004)]**. The Monte Carlo method has been extensively used in the previous decades to precisely estimate dose distributions for clinical beams used in radiotherapy and have become a powerful tool in radiotherapy for dose calculations. Numerous studies have been conducted using these methods for analyzing the influence of linac head components and other factors on the beam's characteristics **[Verhaegen *et al.* (2003), Sheikh-Bagheri *et al.* (2002), Mesbahi *et al.* (2006)].** Therefore, the effect of a flattening filter on photon energy spectrum, the absolute absorbed dose per initial electron, and the beam profile can be studied by using these methods **[Lee *et al.* (1999)]**. In a Monte Carlo (MC) simulation study on Flattening filter free beams, an increased dose rates by a factor of 2.31(6 MV) , 5.45(18 MV) and out-of-field dose reductions were reported **[Vassiliev *et al.* (2006)].**In a similar study, a significant improvement in out-of-field dose was reported for small field sizes **[Titt *et al.* (2006)].** These studies have outlined the possible benefits of removing the flattening filter from beam line. Thus, investigating these properties for a typical modern linear accelerator, such as the Varian Clinic 600 unique performance is important. Our study reports on depth-dose dependencies, the dose rates, the lateral profiles, and the total scatter factors, and the photon and electron fluence in a conventional accelerator and in a flattening filter-free system.

5.2 Material & Methods

5.2.1 Varian Linac Treatment head Simulation Model

To accurately compute photon beam spectra using simulation requires the knowledge of internal structure of linear accelerator along with the characteristics of electron beam hitting the target; in addition there is a need of suitable tool for modeling the linac internal structure.

We have used the BEAMnrc code system to derive best estimates for the mean energy and full width at half maximum (FWHM) of the electron beam incident on the target. Monte Carlo simulations for monoenergetic beams with the energy in the range from 5.5 to 6.2 MeV and FWHM varied from 0.15 to 0.25 cm were performed to find the best match with percentage depth-dose (PDD) and profile measurements. A monoenergetic source with a beam kinetic energy of 5.7 MeV and a FWHM for the X and Y directions of 0.2 cm was found to give best agreement with the measured data. The geometry and materials used to build the Monte Carlo model of the linear accelerator were based on the machine specifications provided by the manufacturer Varian Medical Systems. The linac was structured in the following order: a target slab of tungsten and copper, a primary collimator (tungsten), a flattening filter, an ion chamber, a mirror and jaws (tungsten). All materials used in the MC simulation were extracted from the 700 ICRU PEGS4 (pre-processor for Electron Gamma Shower) cross-section data available in BEAMnrc, and met the specifications for the linac as provided by the manufacturer.

5.2 2. Organization of Monte Carlo simulations

In this section we describe the different stages of simulation for the 6-MV photon beam produced by the Varian linac by using the principal features of the BEAMnrc-DOSXYZnrc code which is shown in figure 5.1. In the simulation of the full accelerator unit, we have split the computations into three steps in order to save time. In the first step, which takes the most computing time, 1.5×10^8 initial histories are simulated, a monoenergetic electron beam source of kinetic energy 5.7 MeV and FWHM for the X and Y directions of 0.2 cm, strike the target. The primary collimator, flattening filter and ion chamber are included in this step. The

output of this step is a phase-space file at plane one as show in figure 5.1, having information on the energy, position, direction, charge and history variables for every particle exiting downstream from the end of ion chamber. Since the source and the primary collimator have fixed openings, this phase-space data may be used for the simulation of different field sizes. This large set of particles produced in the first step is used repeatedly as the input to the next step of simulation. The second step of the calculation simulates the passage of particles through the mirror, adjustable collimator and air slab to a plane for a source-to-surface distance (SSD) of 100 cm from target. We simulated different openings of the adjustable collimator to get field sizes from 5 × 5 to 20 × 20 cm^2 at an SSD equal to 100 cm. The output of this step is a phase-space file at plane two, as show in figure 5.1, having information of the energy, position, direction, charge and history variables for every particle reaching the plane at a SSD of 100 cm from target. The data analysis program BEAMDP is used to analyze the phase space data files to extract the various types of spectra for all particles reaching the plane at a SSD of 100 cm. In the third step of the simulation, the phase-space files for field sizes from 5 × 5 to 20 × 20 cm^2 at SSD of 100 cm, which are obtained at the end of the second step are reused in the DOSXYZnrc code as an input for the dose calculations in a water phantom, as shown in figure 5.1. We transport the particles through a water phantom with dimension of 30 × 30 × 30 cm^3 with a voxels size of 0.25 × 0.25 × 0.25 cm^3. In the **simulation** of **the "unfiltered" 6-MV photon beam,** all three steps of the simulation are same, expect for the first step where the flattening filter is being removed from the beam line. A comprehensive set of dosimetric data for 6-MV filtered photon beams were acquired by using three-dimensional (3D) phantom, Blue phontom^2 IBA Dosimetry GmbH and OmniPro-Accept 7 data acquisition software. All the measurements were performed with a Scanditronix/Wellhofer compact ionization chamber CC13.

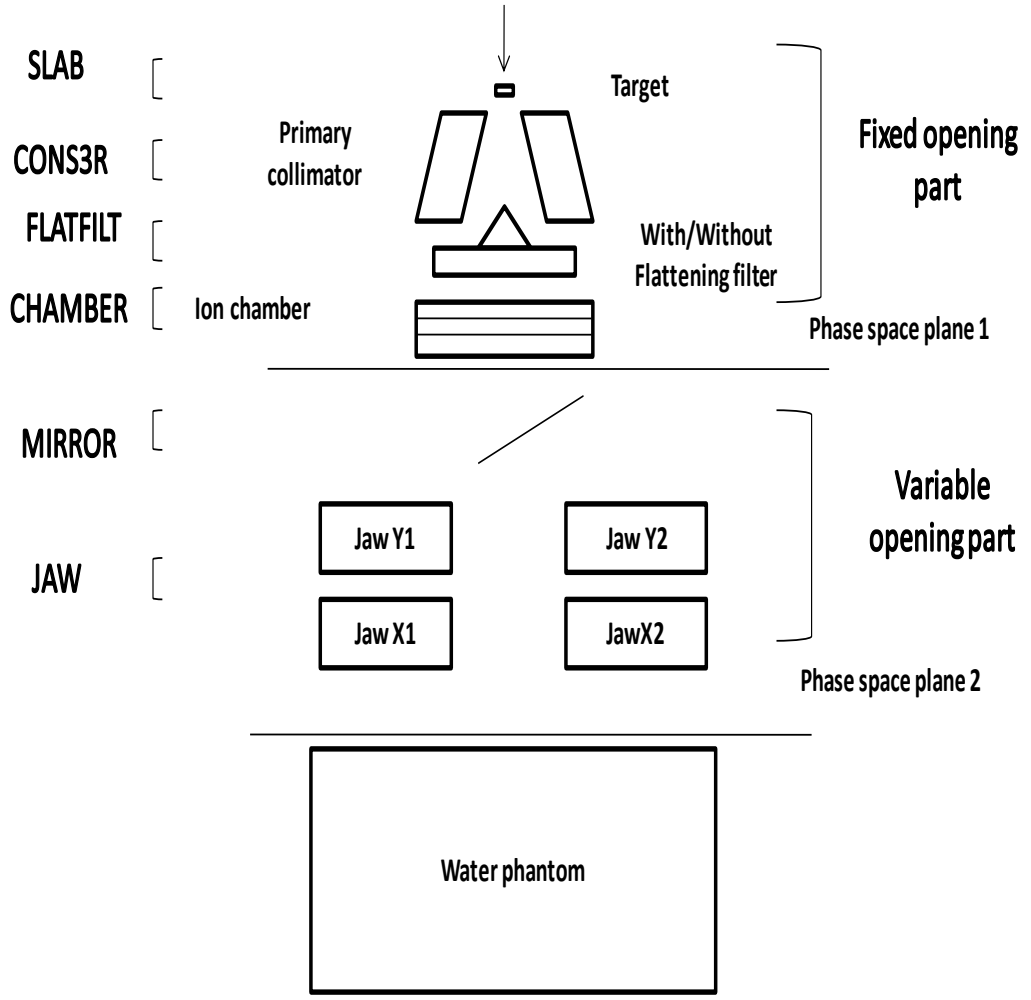

Figure 5.1: 6 MV Varian Linac simulation model separated into three parts, Treatment head fixed and variable Opening part representing first and second step of simulation modelled using component module of BEAMnrc code and Dose Calculation inside water phantom using DOSXYZnrc code in third step .

5.3 Comparison of Monte Carlo simulation Model calculated data with experimentally Measured data for Validation of the simulation model .

5.3.1 Comparison Depth-dose curves

Depth-dose curves for filtered 6-MV photon beams for field sizes from 5 × 5 to 20 × 20 cm^2 were calculated in an on-axis cylinder with a radius of 1 cm by using Monte Carlo

simulations, and compared with the measured data to validate the simulation model. The calculated central-axis depth-dose curves were normalized to unity at the depth, d_{max} of the maximum dose deposition, D_{max}. Both the measured and the calculated results could then be compared with respect to the relative value of the maximum dose D_{max} and the corresponding depth d_{max}. Figure 5.2 shows the comparison between the calculated depth-dose distributions and the measurements for the three different field sizes studied in this work. The comparison showed that the calculated and the measured data agree to within 1% of the local relative dose and to 1 mm in depth at all depths and field sizes which are summarised in Table 5.1.

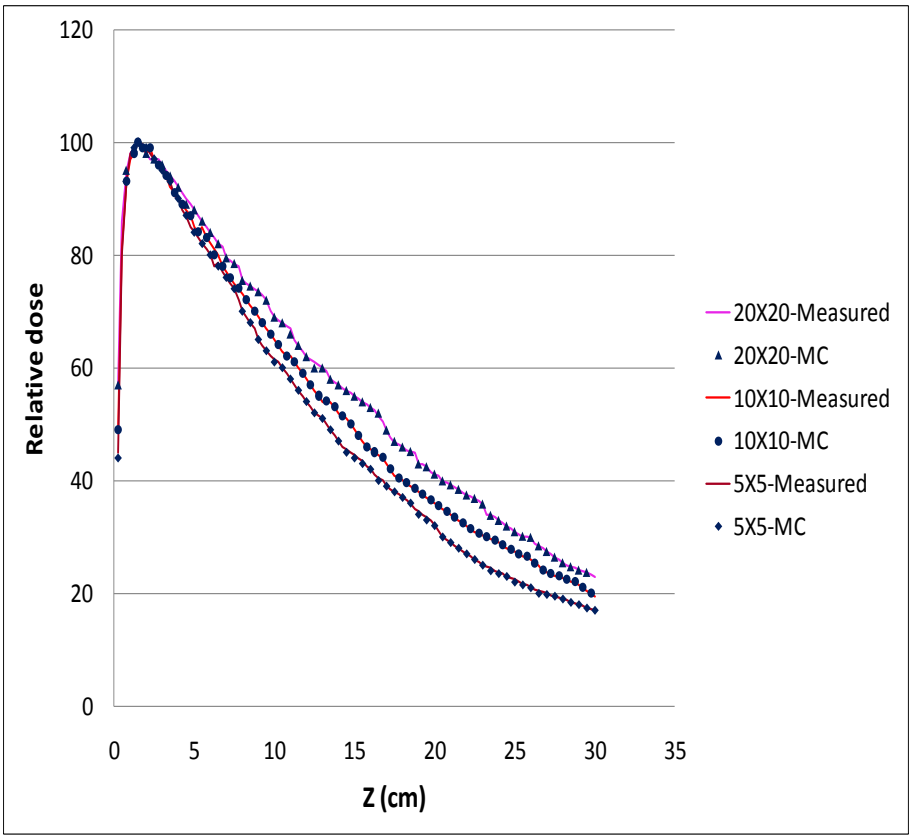

Figure 5. 2: A comparison of measured and calculated depth doses curves of the 6MV photon beam for 20×20, 10×10 and 5×5 cm^2 field sizes .

Table 5.1: Comparison of calculated and measured central-axis depth-dose profiles for different field sizes. A denotes the field size, d_{max} (cm) denotes the location of the maximum Dose, and ΔD_{max} is the relative dose difference between the measurement and the calculations at d_{max}

A(cm^2)	**d_{max}(simulated)**	**d_{max}(measured)**	**ΔD_{max}**
5×5	1.50	1.56	0.20
10×10	1.50	1.52	0.17
15×15	1.48	1.50	0.13
20×20	1.38	1.40	0.10

5.3.2 Comparison Lateral beam profiles

Lateral beam profiles for the filtered 6-MV photon beam were also simulated for field sizes from 5 × 5 to 20 × 20 cm^2 at depths of 1.5, 5 and 10 cm. The measured and the calculated lateral dose profiles were normalized to unity on the central axis for comparison. Figure 5.3 shows the comparison of Monte Carlo calculations to measured data for field sizes of 20 × 20, 10 × 10 and 5 × 5 cm^2 at a depth of 10 cm. The lateral field size at the 50% dose level (X_{50}) and the penumbra widths P_{90-10} and P_{80-20} (calculated from the 90% level to the 10% level and from 80% to 20%) were calculated by using Monte Carlo simulations and compared with experimentally measured data. The results of the comparisons are summarized in Table 5.2. The differences between the measurement and the simulation results for the lateral field size at the 50% dose level, X_{50}, were found to be less than 1 mm.

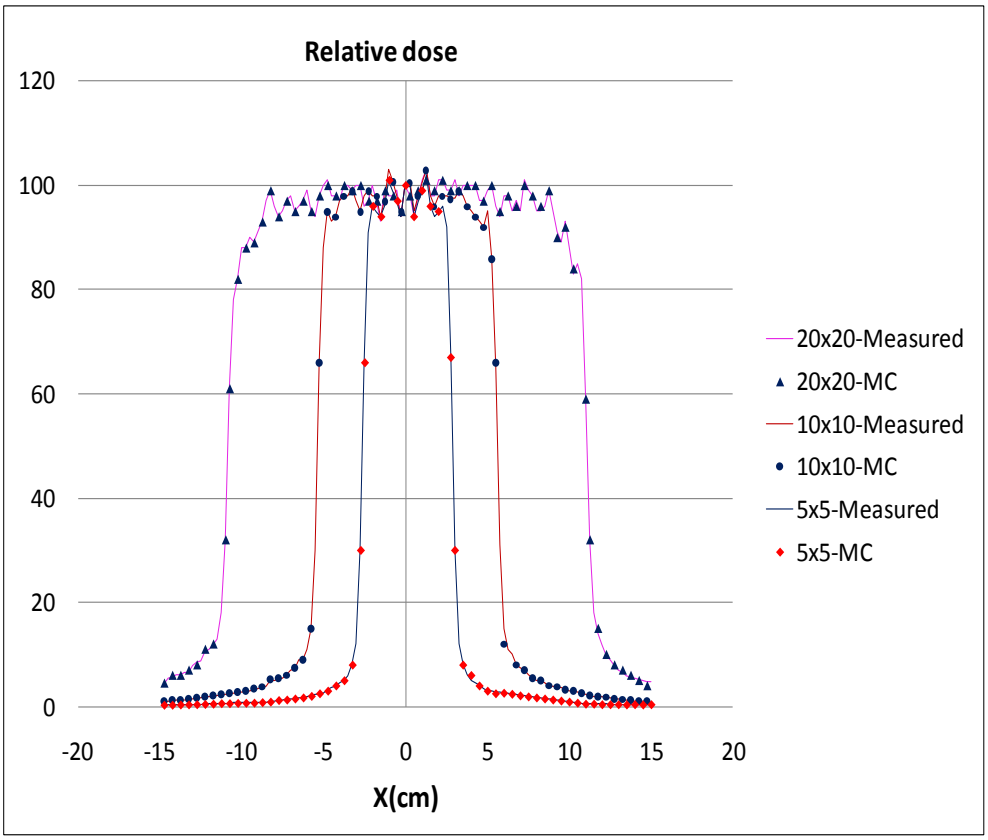

Figure 5.3: A comparison of measured and calculated beam profiles of the 6MV photon Beam at a depth of 10 cm for 20×20, 10×10 and 5×5 cm^2 field sizes.

Table 5.2: Comparison of measured and calculated lateral dose profiles at 10 cm depth. A Denotes the field Size, ΔX_{50} (mm) is the lateral difference measured at the 50% Dose point in the Penumbra, and ΔP_{90-10}(mm) as well as ΔP_{80-20}(mm) describe the Difference in width of the penumbra measured from the 90% point to 10% dose Point and from 80% to 20% Dose point respectively.

A(cm^2)	**ΔX_{50}**	**ΔP_{80-20}**	**ΔP_{90-10}**
5×5	0.10	1.50	0.8
10×10	0.50	1.52	1.0
15×15	0.40	1.20	2.0
20×20	0.50	1.00	2.2

5.4 Simulations without the flattening filter and comparison of unflattened beam Characteristics with flattened Beam

5.4.1 Absolute dose comparison

Absolute absorbed dose per initial electron were calculated for flattened and unflattened beam on central axis. For comparison purposes, we considered the depth of 1.5 and 10 cm as a reference depth for dose rate comparison. The ratios of absolute depth doses for flattening filter free to standard flattened beams were calculated and are presented in Table 5.3. It was observe that absorbed dose per initial electron increased significantly by removing flattening filter, indicating an increased in dose rate for unflattened beam per initial electron. However, the increase in dose rate is decreased with increase in depth.

Table 5.3: Ratios of absolute depth doses for flattening filter free to standard flattened beams at two reference depths for different field sizes . A denotes the field size; d denotes the depth inside water phantom . Absorbed dose calculated without the flattening filter in the beam line is denoted as D_{FFF} (flattening filter free) and with filter in beam line is denoted as $D_{FF.}$

A(cm^2)	$\left(\frac{D_{FFF}}{D_{FF}}\right)$ **At d=1.5 cm**	$\left(\frac{D_{FFF}}{D_{FF}}\right)$ **At d=10 cm**
5×5	2.472	2.420
10×10	2.474	2.400
15×15	2.447	2.440
20×20	2.444	2.380

5.4.2 Percentage Depth-Dose Characteristics

Percentage depth-dose curves **(**PDD) were generated using absolute depth dose values. It can be seen from figure 5.4 that PDDs calculated for unflattened beam is slightly lower than standard beam for all field sizes. Difference in the PDDs of flattened and unflattened beams are evident at deeper depths and are increased with depth for all field sizes studied in our investigation. To verify this difference two parameters are reported in Table 5.4, namely, the Relative dose at a depth of 10 and 20 cm (D_{10}, D_{20}).

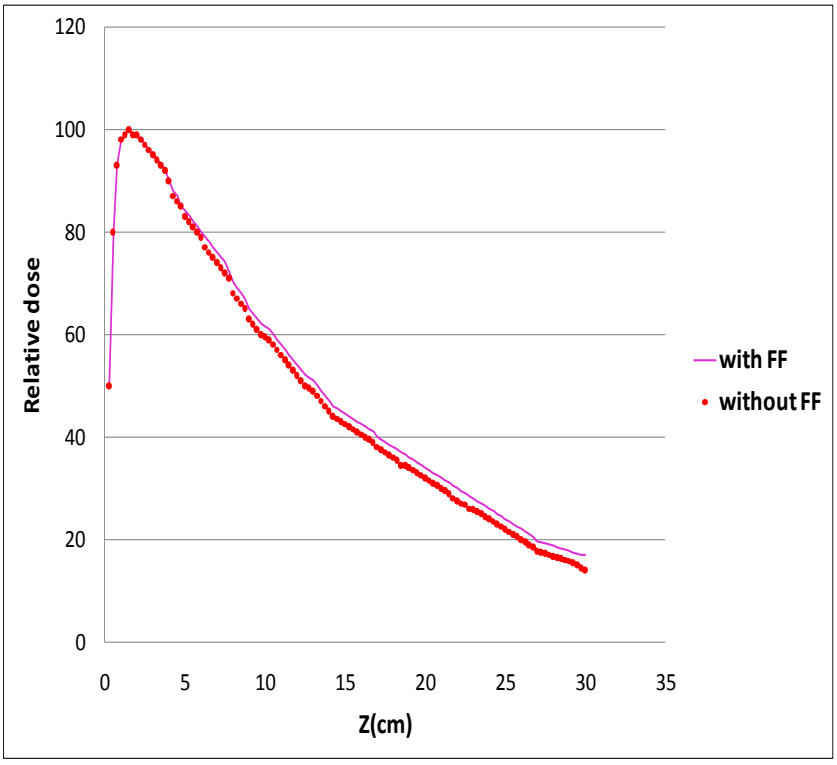

(a)

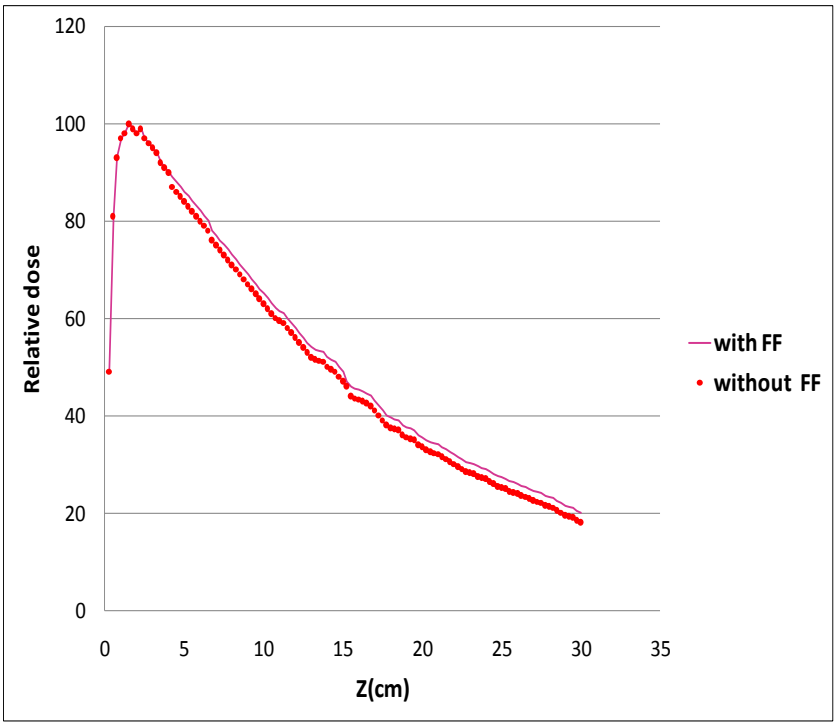

(b)

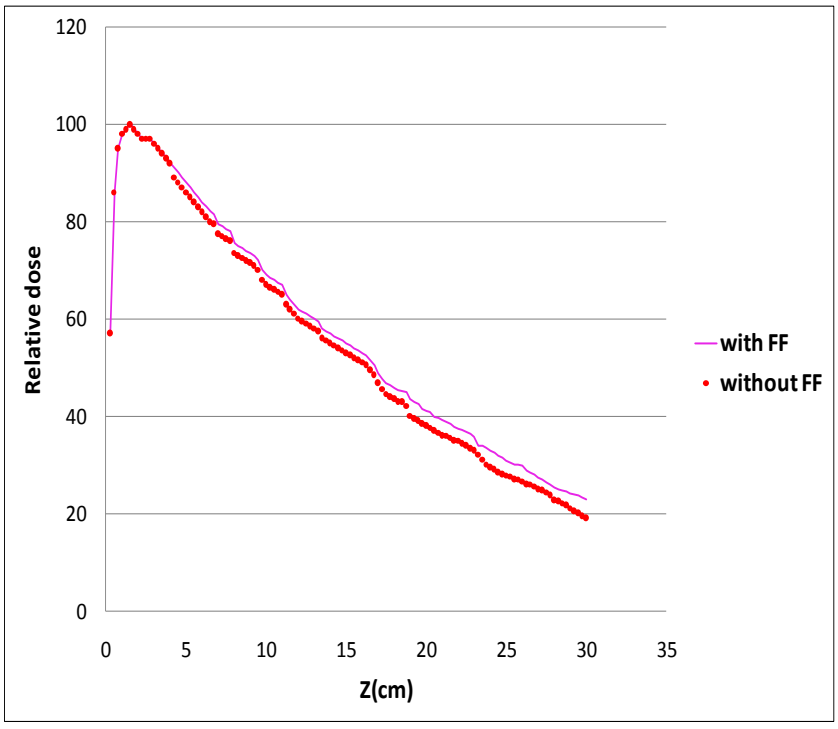

(c)

Figure 5. 4: Comparison of the MC calculated Percentage depth Dose for Flattened and unflattened Beam for Field size **(a)** 5×5 cm^2 **(b)** 10×10 cm^2 **(c)** 20×20 cm^2 Abbreviations: FF denotes flattening filter

Table 5. 4: Comparison of relative depth doses for flattening filter free to standard flattened beams at two reference depths for different Field sizes . A denotes the field size; D_{10} and D_{20} denotes relative depth dose at 10 and 20 cm depth; FF denotes flattening filter.

A(cm^2)	Relative dose at depth of 10 cm D_{10}		Relative dose at depth of 20 cm D_{20}	
	With FF	**Without FF**	**With FF**	**Without FF**
5×5	61.87	59.77	33.14	30.88
10×10	66.67	63.40	37.32	34.50
15×15	68.32	66.49	39.20	36.69
20×20	69.50	64.54	41.60	37.98

5.4.3 Analysis of Spectra of unflattened photon beam

5.4.3.1 Photon Fluence Spectra Variation with Energy

Figure 5.5 shows photon spectra as a function of energy (number of photons per MeV per incident electron on the target) calculated for central axis. Photon emerging from target passes through the components of the collimating system on their way to the scoring plane at an SSD 100 cm. Scoring plane was taken as an annular region around the central axis with radius of 2.25 cm. The range of possible energy of Photon is divided into interval (bin) of 0.25 MeV. The number of photon within each energy bin crossing the scoring plane is being recorded for with and without flattening filter case separately. The precision of calculated

central-axis photon spectra for all the field sizes used in the dose calculations is high and uncertainty in each 0.25 MeV wide bin is usually between 1 to 5%, except for the high-energy end of the spectra. There is an evident increase observed in the photon fluence when the flattening filter is removed from the beam line.

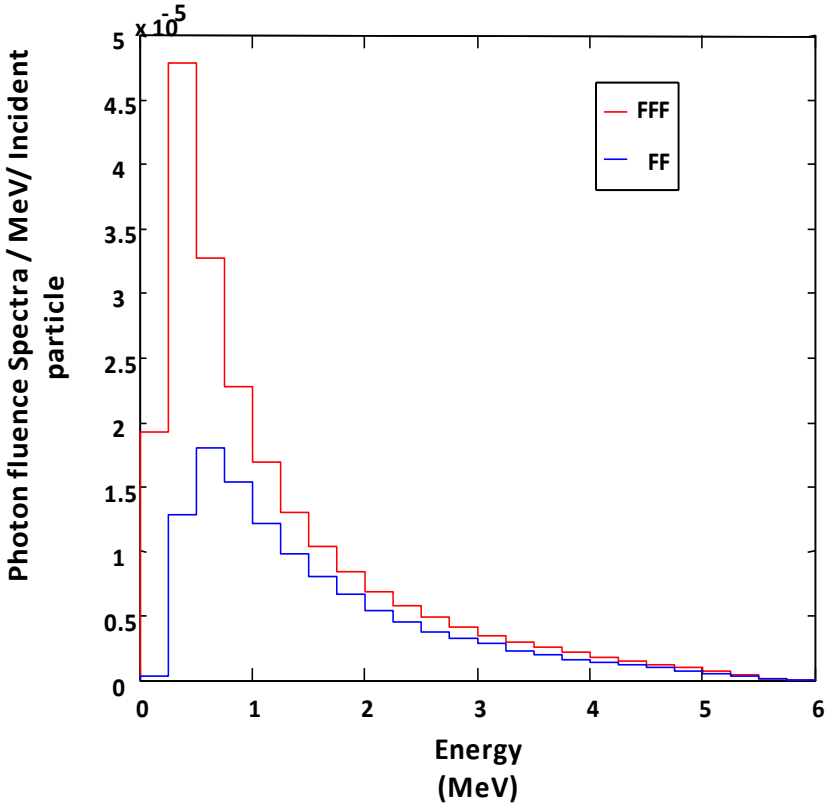

Figure 5.5: Photon fluences per initial electron on the target, at the top of the water phantom as a Function of Photon energy E (MeV) for 20×20 cm^2 field size calculated for with and without a flattening filter in beam line . FF denotes with flattening filter, FFF denotes without flattening filter.

5.4.3.2 Photon Fluences Spectra Variation with off-axis distance

Figure 5.6 shows photon fluences (number of photons per MeV per incident electron on the target) as a function of the off axis distance calculated for a field size of 20 × 20 cm^2.

Photons emerging from the target pass through the components of the collimating system on their way to the scoring plane at SSD of 100 cm. The scoring plane was taken as an annular region around the central axis with radius of 15 cm. The annular region has been divided into equal intervals (bins) of 0.5 cm. The numbers of photons within each bin crossing the scoring plane with and without flattening filter were recorded separately. The precision of the calculated photon fluences spectra for all the field sizes used in the dose calculations was high and the uncertainty in each 0.5 cm wide bin is usually between 1 to 5%, except for the high-energy end of the spectra. For unflattened photon beam increased fluence near the beam central axis was observed.

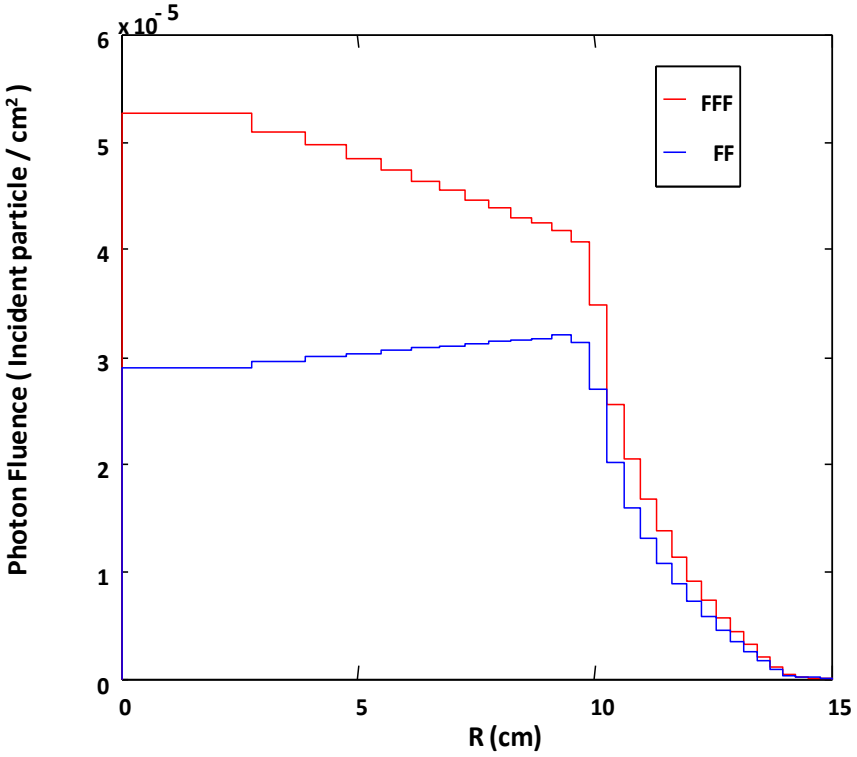

Figure 5.6: Photon fluences per initial electron on the target at the top of the water phantom as a Function of the off-axis distance for a field size of 20 × 20 cm^2 calculated with and Without a flattening filter in the beam line . FF denotes with flattening filter, FFF denotes without flattening filter.

5.4.3.3 Average energy distribution

Figure 5.7 shows the calculated photon average energies distribution at 100 cm SSD for 20×20 cm^2 field size as a function of off axis distance for flattened and unflattened beams. From this distribution we found that the mean photon energy for flattened beam at central axis was 1.52 MeV and decreased to 1.3 MeV at off axis distance of 20 cm. It proves that the beam hardening effect was produced by the flattening filter. For the unflattened beam, the mean energy of spectra was not changed significantly with increasing off axis distance and it was respectively decreased from 1.23 MeV on central axis to 1.19 MeV at 20 cm off axis distance for 20×20 cm^2 field size.

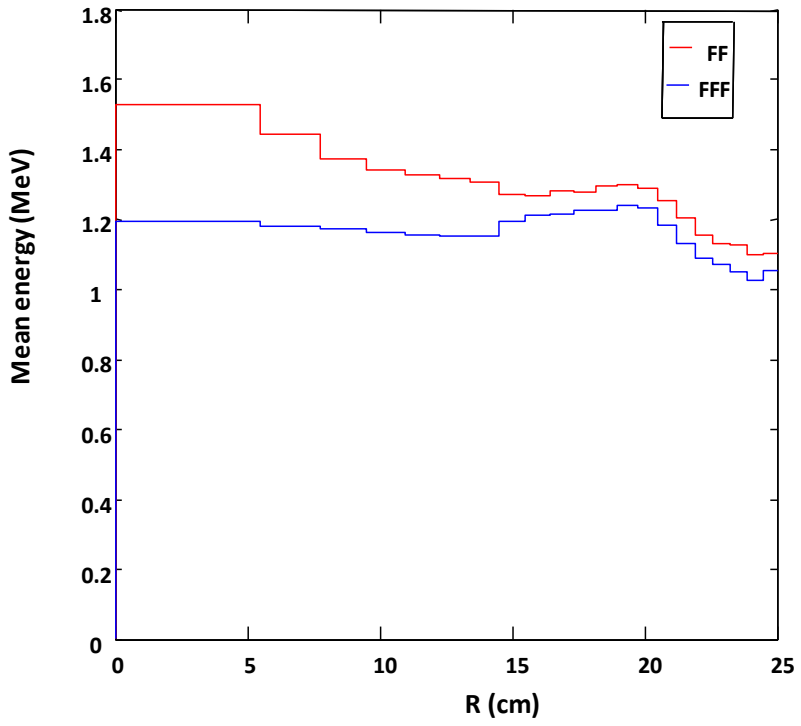

Figure 5.7: Photon average energy distribution of the filtered and unfiltered 6-MV beams as a function of the off axis distance for 20×20 cm^2 field size. FF denotes with flattening filter, FFF denotes without flattening filter.

5.4.3.4 Electron fluence spectra Variation with Energy

The Electron fluence increase indicate a potential risk of delivering an elevated skin dose to the patient and also the risk of placing ion chamber used for the measurement outside the range of its reliable operation. Figure 5.8 shows that the calculated fluence spectra for contaminant electrons calculated for central axis with a radius of 2.25 cm and energy bin of 0.25 MeV at 100 cm SSD for with and without flattening filter case separately. In this study it was found that the number of electron reaching the phantom surface increased by removing the flattening filter from the beam line. The average value of electron fluence spectra calculated for unflattened beam was found to be 1.25 times greater than its value with flattened beam for a field size of 20×20 cm^2.

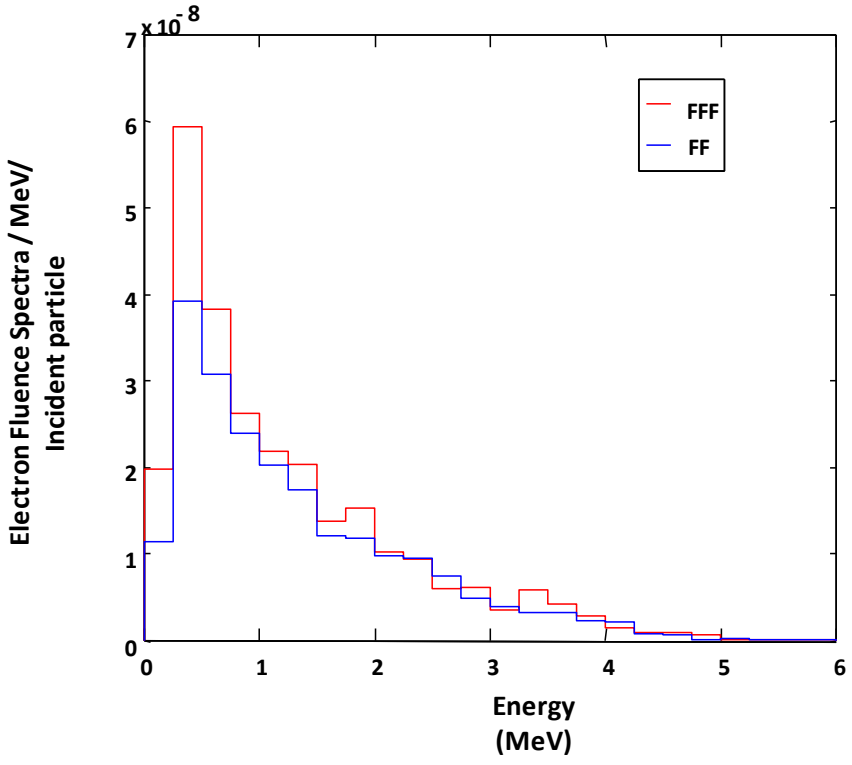

Figure 5. 8: Electron fluences per initial electron on target, at the top of the water phantom as a function of energy E (MeV) for 20×20 cm^2 field size calculated for with and Without a flattening filter in beam line . FF denotes with flattening filter, FFF denotes without flattening filter.

5.4.3.5 Electron Fluence Spectra Variation with off axis distance

Figure 5.9 shows the calculated electron fluence spectra as a function of the off-axis distance for a field size of 20 × 20 cm^2 at a 100 cm SSD for flattened and unflattened beam. In this study, the number of electron reaching the phantom surface was found to be greater when the flattening filter was removed from the beam line. However, the difference between the two cases decreases with increases in the off-axis distances. The MC calculation demonstrated that the electron fluence at the centre of 6-MV unflattened beam was 1.25 times greater than its value with the flattening filter for a field size of 20 × 20 cm^2.

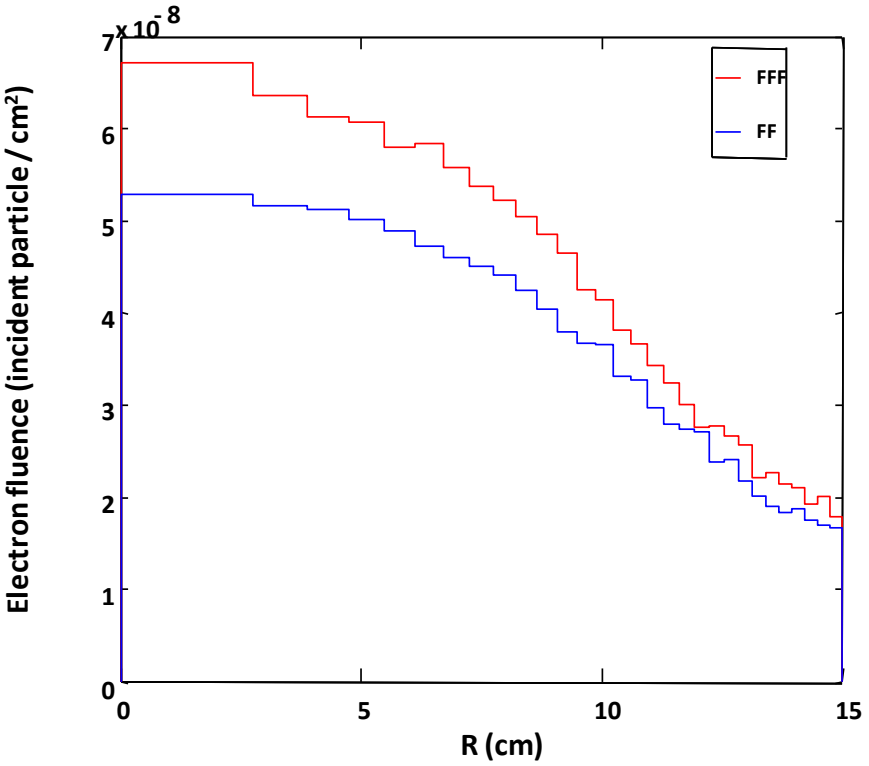

Figure 5.9: Electron fluences per initial electron on target at the top of the water phantom as a Function of the off-axis distance for a field size of 20 × 20 cm^2 calculated With and without a flattening filter in the beam line . FF denotes with flattening filter, FFF denotes without flattening filter.

5.4.4 Surface Dose

Surface dose has been calculated for different field sizes for both with and without flattening filter case and is listed in Table 5. 5. The PDD of first scoring voxels from surface of the phantom with 0.25 cm thickness from the top of water phantom surface was taken as a measure of surface dose. There were differences in doses of build up region between with flattening filter and without flattening filter cases. Surface dose is affected significantly by electrons reaching the phantom surface. Due to the higher fluence of electron in unflattened beam the surface dose was found to be higher than flattened beam for all the field sizes.

Table 5.5 PDDs for first scoring voxels as an indication of the surface dose for different field Sizes.

Field size (cm^2)	**Relative surface dose with Flattening filter**	**Relative surface dose without Flattening filter**
5×5	47.80	53.72
10×10	49.40	56.20
15×15	53.20	59.80
20×20	55.19	63.10

5.4.5 Scatter function

The total scatter factor, S_{CP} is defined as 'the dose rate at a reference depth for a given field size divided by the dose rate at the same point and depth for the reference field size (10 × 10 cm^2). It was measured at SSD = 100 cm and a depth equal to d_{max} of a 10 × 10 cm^2 field for different field sizes. The data for with/without flattening filter case are presented in Table 5.6.

The S_{CP} for the unflattened beams was found to have less value for lager field sizes than that of the flattened beams which indicated a reduced head scatter in unflattened beams compared to the standard flattened beam.

Table 5. 6: Total scatter factor Scp of 6 MV photon beams measured for with and without a Flattening filter in beam line . The Scp was measured at SSD = 100 cm, and at the depth of maximum dose d_{max} of a 10 × 10 cm^2 field size.

Field size (cm^2)	Scp with Flattening filter	Scp without Flattening filter
5×5	0.96	0.97
10×10	1	1
15×15	1.031	1.012
20×20	1.048	1.027

5.4 .6 Comparison of Lateral profile of unflattened beam with the flattened beam

In our simulation study of flattening filter free beams delivered with "conventional" medical linear accelerators, we have removed the conical flattening filter from the beam line. The lateral beam profile thus calculated for unflattened beam with Monte carlo simulation shows extremely different dose profiles when compared with the flattened beams; a profile peaked on the central axis are typical features of unflattened beam as shown in figure 5.10. The result obtained in our study for absolute dose ratio calculation, explained the profile peak of the unflattened beam, as for unflattened beam higher dose is deliver to the central axis. This means that widely used concepts of defining flattened beam parameters would need to be modified in order to adapt their interpretation to unflattened beams, while keeping the main concepts valid for both type of modalities. In our study we have used two standard methods given in literature for the normalization of lateral profile of unflattened beam so that it can be compared with the lateral profile of flattened beam.

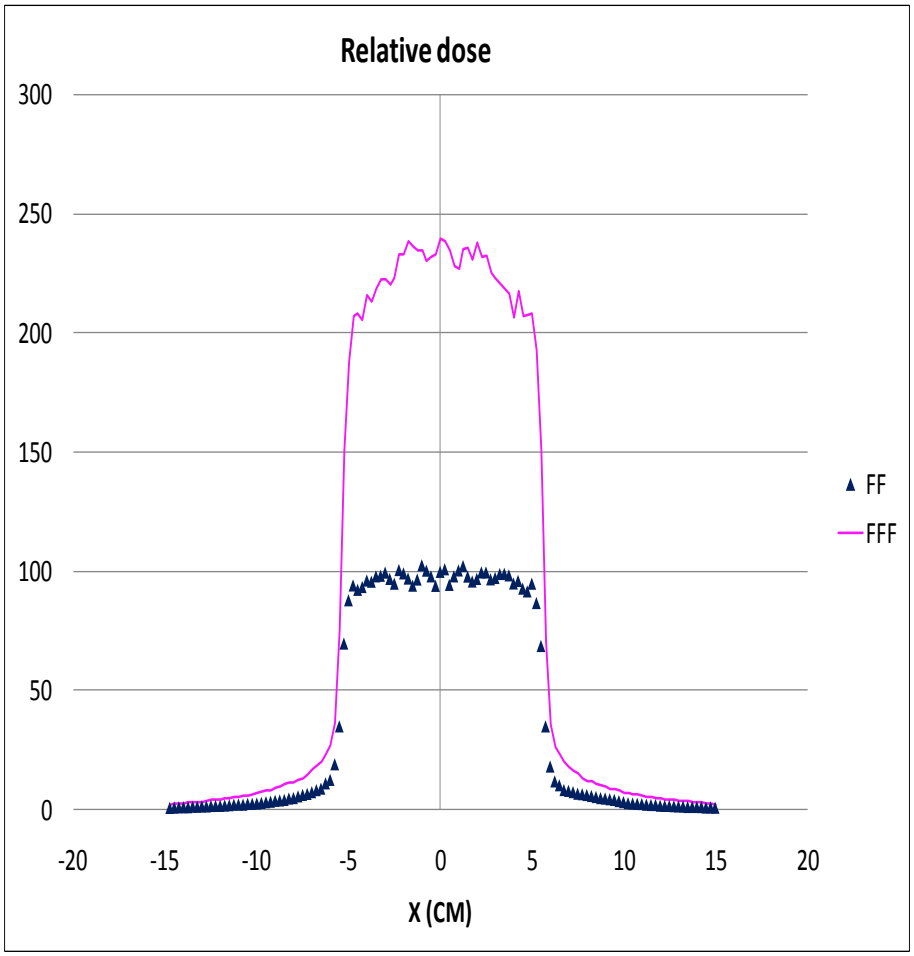

Figure 5.10: Comparison of lateral profile for 6MV photon beams delivered with and Without a flattening filter in beam line at a depth of 10 cm for field size of 10×10 cm^2 . Unflattened beam is normalized by the central axis dose of Flattened beam . FF & FFF denotes for flattened and unflattened Beam.

5.4 .6.1 Unflattened beam lateral profile normalized with Inflection point method

For conventional flattened-beam profiles, the definition of the penumbra is defined as the distance between 20% and 80% dose levels. This is not applicable to the unflattened beam profiles. **Pönisch *et al* [Pönisch *et al.* (2006)]** suggested the use of the inflection point located in the penumbral region to normalize the unflattened beam to the same dose level of a flattened beam. From this normalized profile of unflattened beam it is then possible to evaluate penumbra and the field size according to their usual definition as used for the flattened beam. In our study we have compared the lateral profiles of unflattened and flattened beams for different field sizes. The comparison of the two kinds of beam lateral profiles for field size of 10×10 and 20 × 20 cm^2 at a depth of 10 cm is shown in figure 5.11. For these comparisons, the flat profile is normalized to 1 on the central axis, and the nonflat profile is normalized using the method described by **Pönisch *et al.*** according to which nonflat profile is normalized by dose D_n which was calculated using the following formula:

$$D_n = \left(\frac{D_u}{D_f}\right) * D_{CAX}$$

Where D_u is the dose at the inflection point of penumbra region of the unflattened beam, D_f is the dose at the inflection point of the flattened profile and D_{CAX} is the dose on the central axis of the flattened beam. It was observed in our study that the beam profile for unflattened beam was having relatively lower dose value than the flattened beam near the measured field size edge. The amount of reduction for 10×10 cm^2 field size measured at 4 cm off axis distance was 10% and for 20× 20 cm^2 measured at 9 cm off axis distance was found to be 20% respectively.

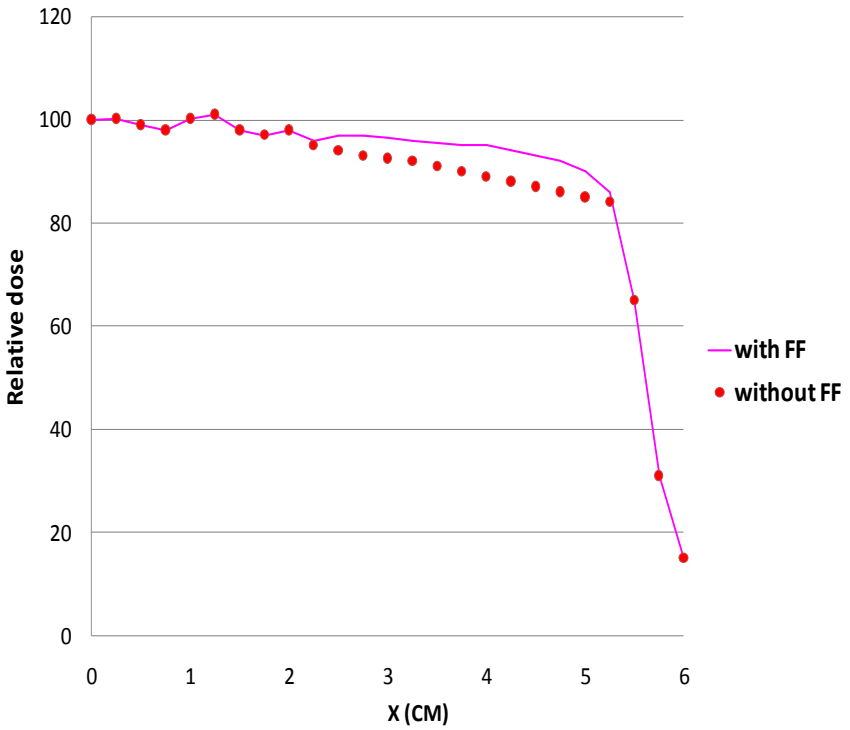

(a)

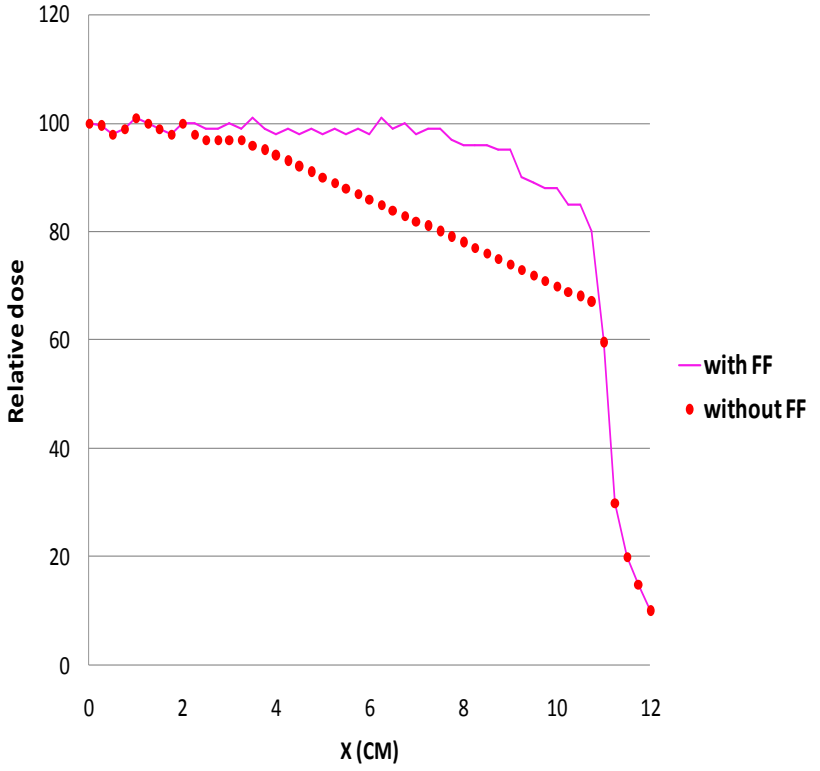

(b)

Figure 5 .11: Comparison of lateral profile for 6MV photon beams delivered for with and Without a flattening filter in beam line at a depth 10 cm for field size **(a)** 10×10 cm^2 **(b)** 20 × 20 cm^2. FF denotes for flattened filter.

The dose in out-of-field region for small field size was also investigated in our study for unflattened beam and compared with that of the flattened beam. Figure 5.12 shows the calculated flattened and unflattened beam profiles for a small field size of 5 × 5 cm^2 calculated at a depth of 5 cm. The dose at 4 cm off-axis distance is lower in unflattened beams by 15% and it tends to decrease faster with increasing off axis distance than in flattened beams. Our results are in consistence with the results reported by **Titt *et.al* [Titt *et.al* (2006)]**. Faster lateral dose fall-off outside the treatment field will result in lower doses to surround normal tissues.

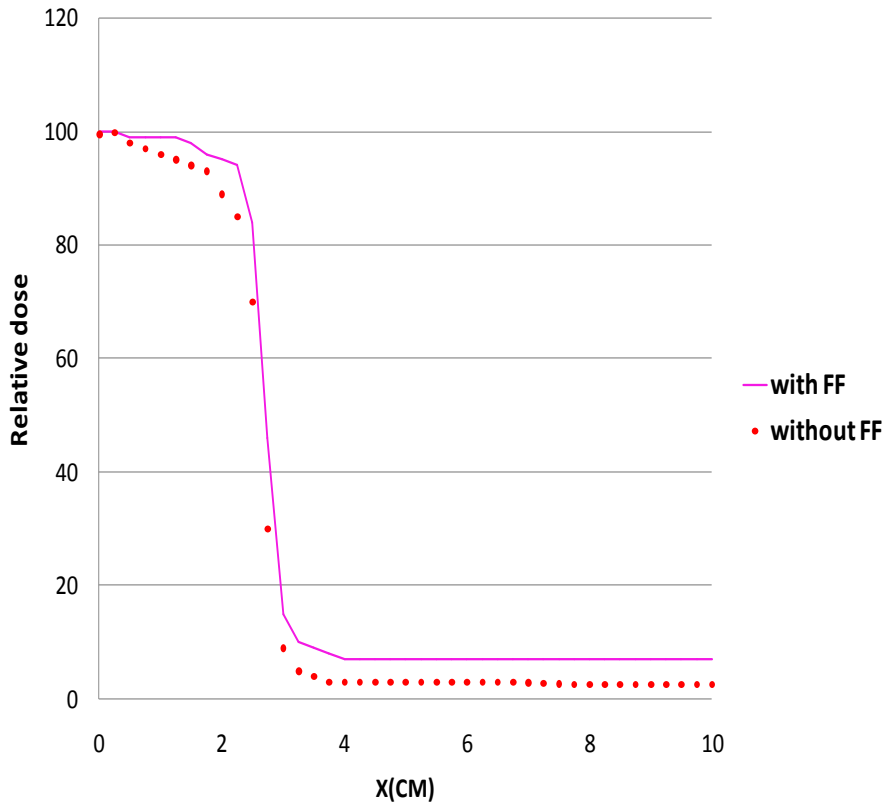

Figure.5.12: Comparison of Lateral dose profiles for a 5× 5 cm^2 field size at a depth of 5 cm. FF denotes flattening filter.

In this study we have computed the beam flatness as the ratio of maximum to minimum dose within 80% of field width for both kinds of beam profiles flattened and unflattened. The comparison of this ratio for both kind of beam is reported in Table 5.7. It was seen that the differences between ratios for the two beams were increasing with increase in field size. It was observed that there was nearly no difference between two cases for small field sizes. These results are in consistence with the results reported by **Jeraj *et al.*** [**Jeraj *et al.* (2004)]**, that the profiles of unflattened beam for field sizes up to 3×3 cm^2 are similar to the flattened beam profiles. Thus, removing flattening filter may have some advantage in radiotherapy techniques, where small field sizes are used. For larger fields, in flattened beams, the ratio was 1.10 or less, whereas in unflattened beams it increased with increasing field size and reached to 1.3 for a 20 × 20 cm^2 field size.

Table.5.7: The ratio of maximum to minimum dose in lateral profiles within 80% of field Size for 6MV photon beams with and without a flattening filter . The profiles Were measured at a depth of 10 cm, at SSD = 100 cm

Field size (cm^2)	$\left(\frac{D_{max}}{D_{min}}\right)$ **With flattening filter**	$\left(\frac{D_{max}}{D_{min}}\right)$ **Without flattening filter**
5×5	1.07	1.04
10×10	1.06	1.16
15×15	1.05	1.20
20×20	1.10	1.30

5.4 .6.2 Unflattened beam lateral profile normalized with Renormalization Method

The inflection point method given by **Pönisch *et al.* [Pönisch *et al.* (2006)]** for normalization of unflattened beam to the same dose level of a flattened beam for computing penumbra and the field size with their usual definition depends upon determination of the inflection point in penumbral region of profile. The straightforward way to determine the position of the inflection point is to plot the dose difference of two adjacent measuring points (ΔD) . The off-axis position of the minimum or maximum at the field edge represents the inflection point. The position of this point is near to the 50% for standard beams normalized to the central axis**,** and is at the highest gradient. This means that the position of the inflection point can be accurately determined only with very fine measuring step size. Together with minute step size and detector size used for measurement in a high gradient region, the dose level that is then used for profile normalization **(according to Pönisch *et al.*)** could be affected easily by an error of 10% or more. On beam central axis this uncertainty value could easily increased for unflattened beam which have dose level of more than twofold with respect to its corresponding flattened beam.

The Renormalization Method

To overcome the uncertainty in the inflection point method, **Fogliata *et al* [Fogliata *et al.* 2012]** purposed renormalization method to determine another normalization point. This method is conceptually similar to the inflection point method and comes to the determination of a point in the "profile shoulder" of flattened beam profiles to renormalize the unflattened beam to the same dose level of the flattened beam at that point. The "shoulder point" is located in a shallow dose gradient region, and in a region where the two unflattened and flattened beams present similar shapes, before the unflattened beams starts to increase in dose

toward the beam central axis. The procedure for determination of normalization point is describe by **Fogliata *et al.*** in the following steps

- The unflattened and the standard flattened beam have to be mutually aligned in the off-axis direction (both centered relative to the central axis).

- Normalize the standard flattened beam as usual to 100% at beam central axis.

- Compute the ΔD from measurements in the penumbra region for normalized flattened beam. This will present two maxima (minima) in the ascending (respectively descending) profile edge.

- The relative dose on the flattened profile corresponding to the off-axis position of the second maximum for the left profile edge (closer to the central axis) (first minimum for the right profile edge) is used to normalize the unflattened beam profile at the same off-axis position

- The relative dose at the unflattened beam central axis is the renormalization value.

After the unflattened beams are renormalized using the above stated procedure the Dosimetric characteristics are evaluated with following definitions:

Dosimetric field size

Once the unflattened beams are renormalized, the concept of dosimetric field size as the distance between the 50% dose levels can be used for unflattened beams, as for flattened beams (generally the full width half maximum (FWHM) is used for standard flattened beams normalized to 100% at central beam axis). Alternatively, as suggested by **Pönisch *et al.*** the distance between the left and right inflection points could be used. But this definition suffers the uncertainty described above.

Penumbra

Penumbra can be defined according to existing protocols, e.g., by the distance between the 20% and the 80% dose levels in the field edge once the profiles are mutually renormalized as suggested above.

Unflatness

The flatness parameter is used for standard beams to evaluate the dose variation within the central beam region, which should be kept minimal for standard flattened beams. This definition is not applicable for unflattened beams thus the shape of the profile has to be characterized by other parameters. **Fogliata *et al.*** proposed the new parameter unflatness to characterize the unflattened beams. Unflatness is the parameter relative to unflattened beams corresponding to the flatness for flattened beams. Unflatness can be defined as the ratio between the dose level at the beam central axis and the dose level at a predefined distance from the central axis as a function of field size,

$$\text{Unflatness} = \frac{\text{Dose}_{\text{central axis}}}{\text{Dose}_{\text{X off-axis}}}$$

Here the numerator is the central axis dose level and the denominator is the dose level at a certain off-axis position X. The off-axis point X was chosen to be located at 80% of the field size (Fs) for Fs ≥ 10 cm and 60% of the field size (Fs) for Fs < 10 cm.

Profile Comparison

In the present study beam profiles for different field sizes were calculated at depths of 1.5 and 10 cm for both flattened and unflattened beams in a water phantom. The lateral profiles of the unflattened and the flattened beams for a field sizes of 5 × 5, 10 × 10 and 20 × 20 cm^2 are compared at a depth of 10 cm as shown in figure 5.13. For above comparison unflattened beam profile is normalized by method described by **Fogliata *et al.*** and flattened beams were normalized at central axis. The main characteristics of the unflattened photon beams in terms of the dosimetric field size, the penumbra and the unflatness calculated at two different depths for three field sizes are presented in Table 5.8.

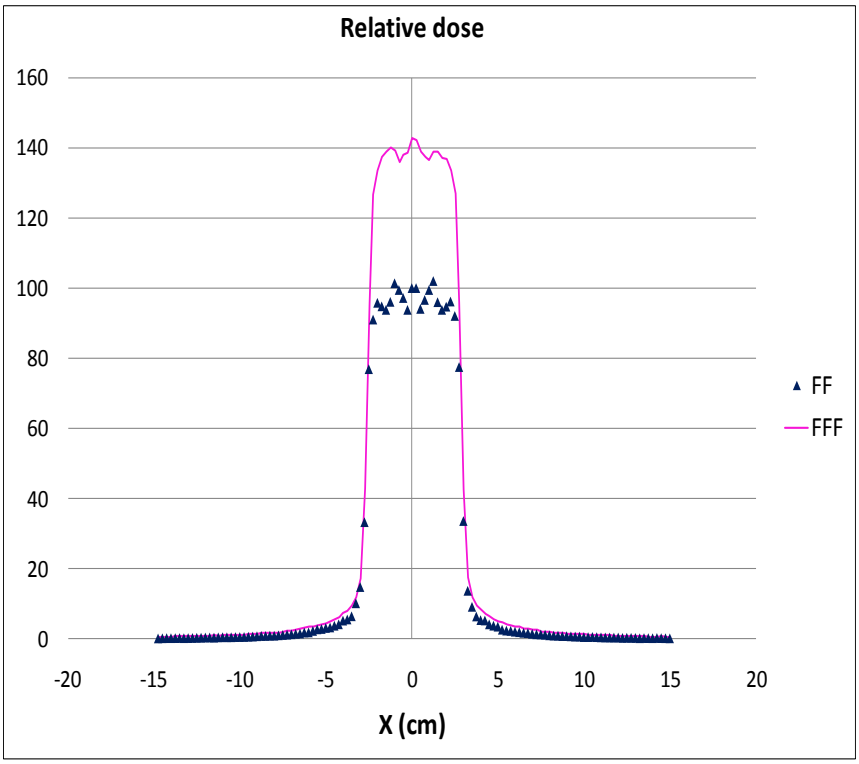
Relative dose
160
140
120
100
80
60
40
20
0
-20
-15
-10
-5
0
5
10
15
20
X (cm)
FF
FFF

(a)

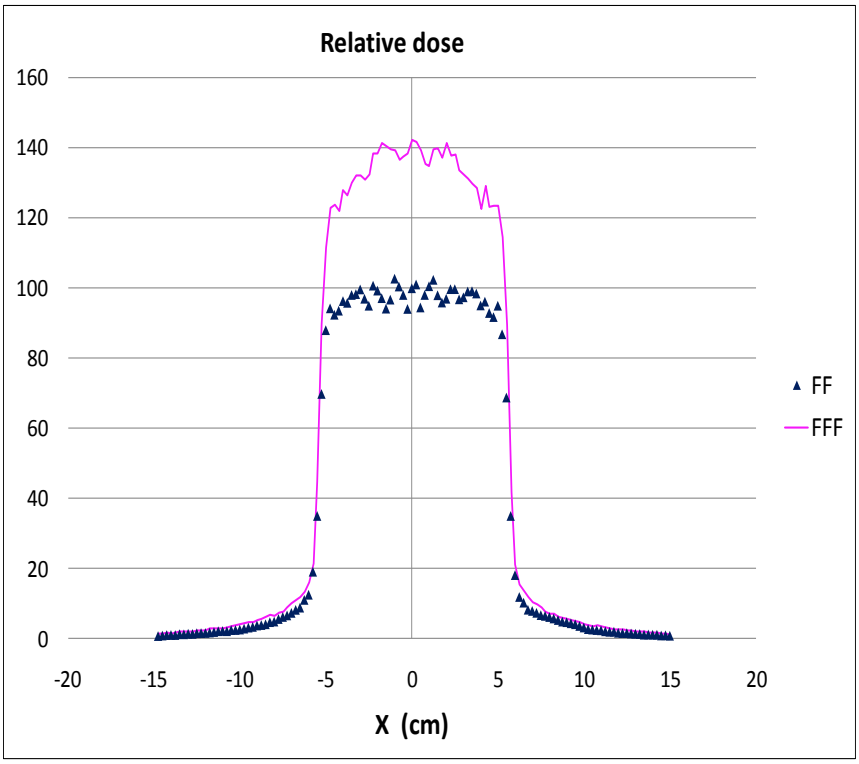
Relative dose
160
140
120
100
80
60
40
20
0
-20
-15
-10
-5
0
5
10
15
20
X (cm)
FF
FFF

(b)

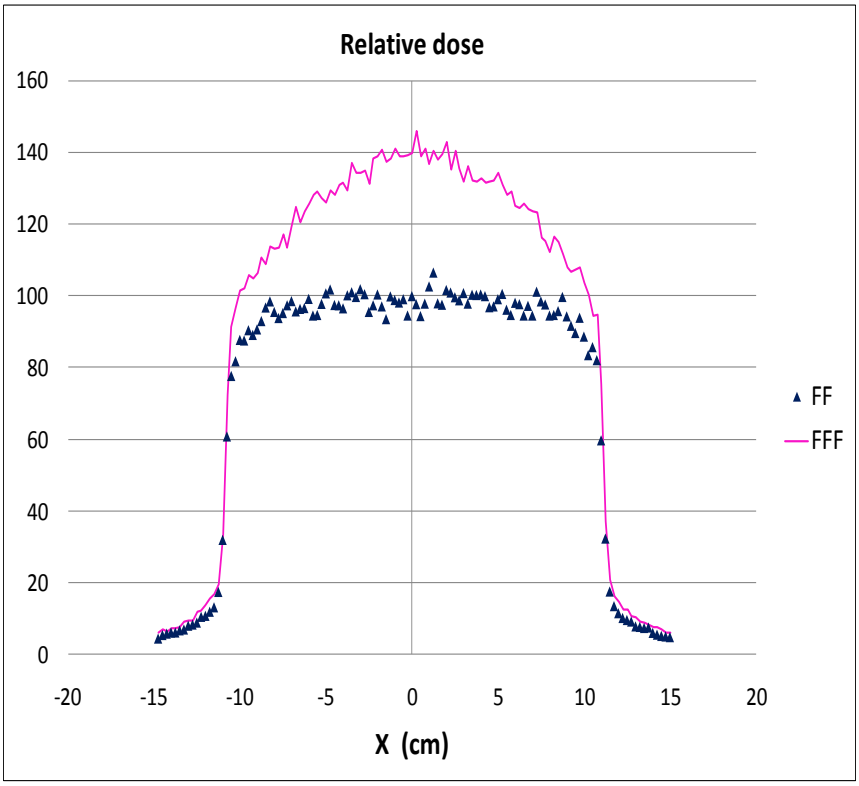

(c)

Figure.5.13: Comparison of the lateral profiles for 6-MV photon beams with and without a flattening filter at a depth of 10 cm for field size of **(a)** 5×5 cm^2 **(b)**10 ×10 cm^2, and **(c)** 20 × 20 cm^2. FF denotes with flattening filter, FFF denotes without flattening filter.

Table.5.8: Profile parameters for unflattened 6-MV photon beams. Data were calculated at SSD = 100 cm. d denotes the depth inside the water phantom.

	Field size (cm^2)		
	5×5	**10×10**	**20×20**
MC-calculated field size (cm)	d = d_{max} 5.06 [-2.43, +2.63] d = 10 cm 5.63 [-2.63, +3.0]	d = d_{max} 10.10 [-5.04, +5.06] d = 10 cm 11.06 [-5.56, +5.50]	d = d_{max} 20.12 [-10.04,+10.08] d = 10 cm 22.08 [-10.98,+11.10]

MC-calculated penumbra (cm)	$d = d_{max}$ 0.20 d = 10 cm 0.43	$d = d_{max}$ 0.23 d = 10 cm 0.53	$d = d_{max}$ 0.27 d = 10 cm 0.76
MC-calculated unflatness	$d = d_{max}$ 1.02 d = 10 cm 1.05	$d = d_{max}$ 1.06 d = 10 cm 1.16	$d = d_{max}$ 1.23 d = 10 cm 1.24

5.5 Discussion & Conclusion

In conventional clinical linear accelerators, a large portion of primary photons especially those close to the central axis of the beam are removed or scatter by the flattening filter, increasing the beam on time and out-of-field exposure of patients. Therefore, removing the filter from the beam line should result in a substantial increase in the dose rate and decrease in the beam on time should be achieved when radiation treatment is delivered. In our study of flattening filter free beams, we investigated theses effects by calculating the absolute absorbed doses per initial electron for the flattened and the unflattened beam at two different depths for different field sizes. The ratios of the absolute depth doses for unflattened beam to those for the standard flattened beam calculated for a field size of 10 × 10 cm^2 at a 10 cm depth at 100 cm SSD was found to be 2.4, indicating a possible higher dose rate was delivered by the unflattened beam. PDDs calculated for the unflattened beam were found to be slightly lower than those calculated for standard beam for all field sizes. The difference between the PDDs of the flattened and the unflattened beams became more evident at deeper depths and increased with increase in depth for all field sizes.

In our investigation of spectral characteristics of unflattened beam, we calculated the photon fluence spectra variation with energy. It was observed that the fluence of photon on central

axis averaged over the total surface of the top of water phantom increased more than twofold with removing flattening filter, explaining the higher central axis dose rate deliver by the unflattened beam. The comparison of photon fluence spectra variation with off axis distance calculated for 20×20 cm^2 field size for the two kinds of beam modalities showed the increment in the photon fluence for the unflattened beam; however, the difference in the photon fluence decreases with increase in off-axis distance.

Average energy distribution as a function of off axis distance for flattened and unflattened beams were calculated in our study. It was observed that for flattened beam the average energy of photon showed variation with off-axis distance. In addition the energy spectrum became softer for the unflattened beam as the average energy of the photon on central axis calculated for a field size of 20×20 cm^2 at a 100-cm SSD at the top of the water phantom decreased from 1.52 to 1.23 MeV for the unflattened beam .This was due to the differential attenuation of the flattening filter with distance from central axis of the beam. The thick central part of the flattening filter attenuates more low energy photons, but as the off-axis distance increases, more low-energy photons are allowed to penetrate the thin lateral part of the flattening filter, and they contribute to the photon energy spectrum; thus, the mean energy of the spectrum is decreased. For the flattening-filter-free beam, the mean energy of the spectrum did not change significantly with increasing off-axis distance and it decreased from 1.23 MeV on the central axis to 1.19 MeV at an off-axis distance of 20 cm for a field size of 20×20 cm^2.

The average energy difference on the central axis is the major cause for the superficial dose difference delivered by the two kinds of beams. The surface dose comparison showed higher dose value for the unflattened beam with respect to flattened beam for all field sizes. The lower average energy of the unflattened beam on the central axis produces a higher

superficial dose since the unflattened beam have higher concentration of low energy particles which are being removed by the flattening filter in flattened beam.

Surface dose calculated for different field sizes for the unflattened beam do not show field size dependence as seen for the flattened beam. The field-size dependence of the superficial dose for the flattened beam was due to the presence of scatter component, which originates mostly from the flattening filter.

Our computation of the total scatter factor, S_{CP}, for the unflattened and flattened beam showed that the value of S_{CP} for the unflattened beam increase more slowly with increase in field size in comparison to as it does for the flattened beam. The forward-peaked profile of the unflattened beam produces a lower S_{CP} because of the reduced off-axis intensity. The flattening-filter-free beam has a greatly reduced fluence at off axis; hence, less secondary head scatter is created, which is directed toward the central axis. For this reason, as the measured field size increases, the increase in the value of S_{CP}, is not seen for the unflattened beam which is found with the flattened beams.

In our study of flattening filter free beam characteristics we computed the lateral profiles of beam for different field sizes and depths. The forward-peaked profile with significantly reduced off axis fluence make the lateral dose profile of unflattened beam extremely different with respect to the flattened beam, making the comparison of two kind of beam profiles very difficult. We have normalized unflattened beam profile with different methods and thereafter compare them with the corresponding flattened beam profiles. The comparison of unflattened beam normalized with the method described by **Pönisch *et al.* [Pönisch *et al.* (2006)]** with flattened beam showed that for both kind of beams the calculated flatness were not significantly different for small field sizes. Thus Beam non flatness is unlikely to present a problem for treatments with small fields and the treatments can also benefit from an increased dose rate, however, for lager field sizes there was a significant difference in beam flatness for

the two cases. Near the field edge of lateral profiles, relative dose values were found to be inferior for the unflattened beam in comparison to the corresponding flattened beam. Since the flattening filter raise the relative fluence of primary photons travelling towards off-axis and more amount of head scatter present in flattened beam, there relative dose values were found to be superior in comparison to the unflattened beam. For unflattened beam the relative dose value calculated outside the field edge were found to be smaller for small field sizes when compared to the flattened beam. In addition out-of-field dose from the flattening filter free beam falls off faster with increase in off-axis distance. Thus a considerable decrease in out-of-field dose and enhanced sparing of normal tissues and organs close to small treatment fields can be achieved.

Fogliata *et al.* described new concept and definitions to identify the characteristics of unflattened beam profile. In our comparative study of unflattened and flattened beam profile, where the unflattened beam profiles were normalized by the method suggested by **Fogliata *et al.*** showed that for unflattened beam the calculated dosimetric field size appear to be smaller than corresponding flattened beam. The maximum decrease was 1.2 mm for a field size of 20×20 cm^2 at a 10-cm depth, however for small field sizes this difference was even more less. The penumbras calculated for the lateral profile of the unflattened beam were found to be smaller in comparison to the corresponding flattened beam. Though increases in the penumbra values with increasing field size were observed for both the flattened and unflattened beam. The measured value of unflatness for the flattening filter free beam showed that the beam non flatness is unlikely to present a problem for treatments delivered for small fields, but for lager field sizes, a considerable increases in its value suggest difference with the flattened beam. Our study of unflattened beam lateral profile normalized with different methods suggests that for small field size there is no significant difference between the

unflattened and flattened beam; and the treatments could also be benefited with increased dose rate.

This chapter was purely focused on the simulation study of flattening filter free beam produced by Varian Clinic 600 unique performance linac after removing the flattening filter from beam line in our simulation model (this machine does not have unflattened mode and operates only in flattened mode). All the calculations were made for jaw define field sizes only for both flattened and unflattened mode of beam delivery. Our study showed that removing flattening filter increases the photon fluence considerably and consequently the dose rate. Reduced dependence of total scatter factor, S_{CP} on field size signifies the decrease in the amount of head scatter present in the unflattened beam. Study of unflattened beam lateral profile normalized with different methods show lower relative dose value and faster rate of decline for them in comparison to flattened beam. These comparative results obtain in our study indicate a reduced out-of field exposure and improved sparing of surrounding tissue and organ other than targeted for radiation treatment.